Mora Mora, MTC.; Rodríguez Álvarez, MJ.; Romero Bauset, JV. (2008). New pixellation scheme for CT algebraic reconstruction to exploit matrix symmetries. Computers and Mathematics with Applications. 56(3):717-726. doi:10.1016/j.camwa.2008.02.019.

New pixellation scheme for CT algebraic reconstruction to exploit matrix symmetries

Cibeles Mora[a], María José Rodríguez-Álvarez[b,*], José Vicente Romero[b]

[a] *Instituto de Física Corpuscular of Valencia, Edificio Institutos de Investigación, 22085 Valencia, Spain*
[b] *Instituto de Matemática Multidisciplinar of the Universidad Politécnica de Valencia, Edificio 8G, Piso 2, 46022 Valencia, Spain*

Abstract

In this article we propose a new pixellation scheme which makes it possible to speed up the time of reconstruction. This proposal consists in splitting the field of view of the scanner into as many circular sectors as rotation positions of the detector. The sectors are pixellated using circular pixels whose size is always smaller than the resolution needed. The geometry of the pixels and the arrangement on circular sectors make it possible to compute the entire matrix from only one position of the scanner. Therefore, the size of the matrix decreases as many times as the number of rotations. This results in a significant reduction of the system matrix which allows algebraic methods to be applied within a reasonable time of reconstruction and speeds up the time of matrix generation.

The new model is studied by means of analytical CT simulations which are reconstructed using the Maximum Likelihood Emission Maximization algorithm for transmission tomography and is compared to the cartesian pixellation model. Therefore, two different grids of pixels were developed for the same scanner geometry: one that employs circular pixels within a cartesian grid and another that divides the field of view into a polar grid which is composed by identical sectors, with circular pixels too.

The results of both models are that polar matrix is built in a few seconds and the cartesian one needs several hours, the size of the matrix is significantly smaller than the circular one, and the time of reconstruction per iteration using the same iterative method is less in the polar pixel model than in the square pixel model. Several figures of merit have been computed in order to compare the original phantom with the reconstructed images. Finally, we can conclude that both reconstructions have been proved to have enough quality but, the polar pixel model is more efficient than the square pixel model.

Keywords: CT mathematical modelling; ART reconstruction; Polar-coordinates; System matrix; Rotation symmetries

1. Introduction

The first reconstruction algorithm approach for CT image reconstruction was based on Algebraic Reconstruction Techniques (ART). The reconstruction problem was modeled by means of a set of linear equations which are resolved

* Corresponding author.
E-mail addresses: cibeles.mora@ific.uv.es (C. Mora), mjrodri@imm.upv.es (M.J. Rodríguez-Álvarez), jvromero@imm.upv.es (J.V. Romero).

by using ART algorithms. Since the system matrix (SM) was the core of ART methods, the SM relates the resulting images and the acquired data and reflects the scanner behavior. The SM size was pretty big and tricky to be handled for the computers of the early 70s. In fact, the images from these scans took 2.5 h to be reconstructed by means of ART on a large computer. Despite all this, the informatics field growth was spectacular, the CT scanner hardware was developed at a more rapid pace. After the first production of X-ray CT machines called the EMI-Scanners [1], several scanner generations followed one after another, and they provided more sensitive detectors, more sophisticated scanner configurations, improved X-ray sources and better hardware acquisition developments. The quantity of data continued growing too, and the ART methods were substituted by Fourier based algorithms [2], which do not use an SM and provided a better reconstruction speed.

However, ART provided a better quality reconstruction than other alternatives, such as filtered back-projection techniques, with incomplete or noisy measurement [3,4].

The popularity of the iterative reconstruction methods started with the Maximum Likelihood Emission Maximization (MLEM) algorithm which was proposed for emission tomography and described in the seminal paper of Shepp and Vardi [5]. Lately, several derived procedures have been proposed such as the MLEM algorithm for transmission tomography [6] and alternative implementations such as the Ordered Subset Expectation Maximization (OSEM) algorithm [7] in which the iterations are accelerated. Therefore, ART methods came to have practical use.

Despite improvements in the reconstruction algorithm, the size of the collected data is one of the drawbacks on these techniques. Several pixellation configurations have been proposed in order to decrease the computational complexity and to improve the reconstruction quality using alternative models such as polar pixels [8,9], blobs grids [10], natural pixels [11] or strip functions [12]. Furthermore, several approaches are based on polar pixel grid for Compton-camera [13], SPECT [8,14,15] and commercial CT [16]. In this paper, two approaches of the mathematical model for a medical CT scanner based on geometric features are proposed. One model is based on using a cartesian arrangement of the pixel and another model is based on a polar arrangement.

(1) The cartesian model is similar to the most usual models used in CT reconstruction but, in this approach the pixels are defined as circles in order to facilitate the calculations.
(2) The polar approach uses an innovative pixellation configuration that takes advantages of all the natural symmetries of the scanner geometry and allows us to reduce the matrix size highly. The polar pixel adds an extra complexity to the reconstruction algorithm and the image visualization. The balance between the properties of the new pixellation configuration and the increased complexity of the polar pixel configuration is evaluated in this paper. The pixels used in the polar pixel model are circular pixels too.

The comparison between these models is of interest, since it helps us to find out if the objective of reducing the size of data by means of a new polar model is accomplished without loss of accuracy in the reconstruction.

This paper is organized as follows. In Section 2, the mathematical model assumptions considered in both models are presented. The cartesian model is described in Section 3 and the polar pixel model in Section 4. The polar grid design criteria, the SM structure and the image visualization in the polar pixel model, are detailed in Section 4. The main features of the reconstruction algorithm MLEM and the implementation details for both models are described in Section 5. Once the models are described, experimental proofs are developed in order to assess the reconstructed images of both models by means of quality indicators. The CTSim simulation package [17] has been chosen in order to obtain a simulated data acquisition because this is a free package that allows us to compare our methods, easily. These details about the implementation of the model and the figures of merit definition are presented in Section 6. The results of the implementation using this simulated data source and the figures of merit are given in Section 7. The objective of this section is to resume the comparison between both models in terms of efficiency and reconstruction quality. Finally, several conclusions about the model and their implementation results are given in Section 8.

2. Basis of mathematical model for a CT scanner

The reconstruction is the process whereby the acquisition data becomes a reconstructed image which reflects the original object. In ART algorithms, the relation between images and acquired data is modeled by means of the SM elements. Therefore, the properties of the reconstructed image are determined by the SM model and the reconstruction algorithm.

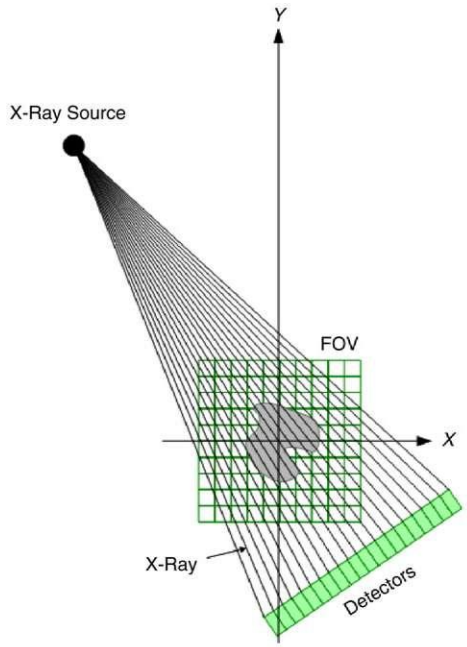

Fig. 1. The figure shows a fan-beam scanner in which the detectors, X-ray source, ray projections and field of view are marked.

Here, a mathematical model of a 2D scanner is proposed based on the following points:

- If the scanner system is a fan-beam CT scanner geometry defined by an X-ray source and a 1D array pixellated detector (see Fig. 1), a ray is the area delimited by the X-ray source and the two lateral limits of each detector element which shapes a triangle.
- The scanner measurement is composed by several rotated positions around an isocenter point. The Field of View (FOV) is the intersected area delimited by all the scanner positions, in which the measured object is located. The area of the reconstructed images is the result of a FOV discretization.
- In this model, the pixels are defined as circles which are arranged in two configurations, one in a cartesian grid and another in a polar grid.
- An element w_{ij} of the system matrix W, is defined as the circular pixel j area which intersects a ray beam i as shown in Fig. 2. The circular shape of the pixel is chosen because its symmetries simplify the calculation of areas. Actually, the symmetry of circular pixels makes it possible to reduce the calculation of areas to only six different cases for all different rays and views of the focus. Fig. 2 shows an example of one of these cases.

3. Square grid model

In the square pixel model the circular pixels are arranged into a cartesian grid as shown in Fig. 3. This figure shows the pixel alignment of the model and a magnification of a pixel j in which is shown the definition of a weight element w_{ij} as the area intersected in pixel j by a ray i.

Since the pixel configuration is cartesian, the reconstructed images can be visualized directly. Despite the fact that the circular pixels are perfectly symmetric from all the scanner rotated locations, the square pixel model has only 4 symmetries due to the arrangement in a cartesian grid which are marked in Fig. 3.

4. Polar grid model

4.1. Circular pixels in a polar grid

The focus of the polar pixel model has been to maintain at least as good quality features as the square pixel model and to provide more symmetries to the SM. Using both criteria, the design of this pixel grid has been tackled using

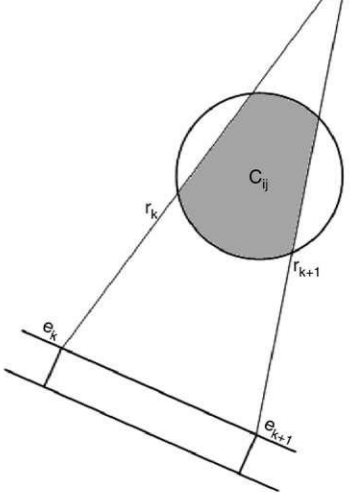

Fig. 2. The figure shows a pixel j overlapped by a ray i. The SM weight w_{ij} is the shady area which intersects the ray and the pixel.

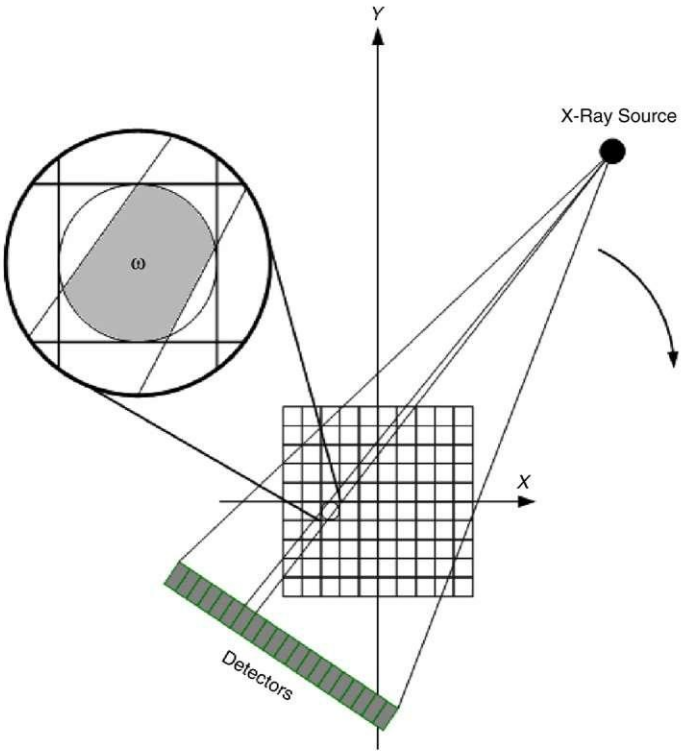

Fig. 3. The Square Pixel Model is shown for a simplified example of 20 detectors and 100 pixels.

two main principles: to preserve the intrinsic spatial resolution of the scanner and to take advantage of all the natural symmetries that the scanner geometry provides in order to compact the SM. Therefore, it was decided to design the pixel grid by dividing the FOV into v equal circular sectors (see Fig. 4). Each circular sector is divided into pixels following a similar distribution to the one shown on Fig. 5. As a result, the pixel configuration observed from the

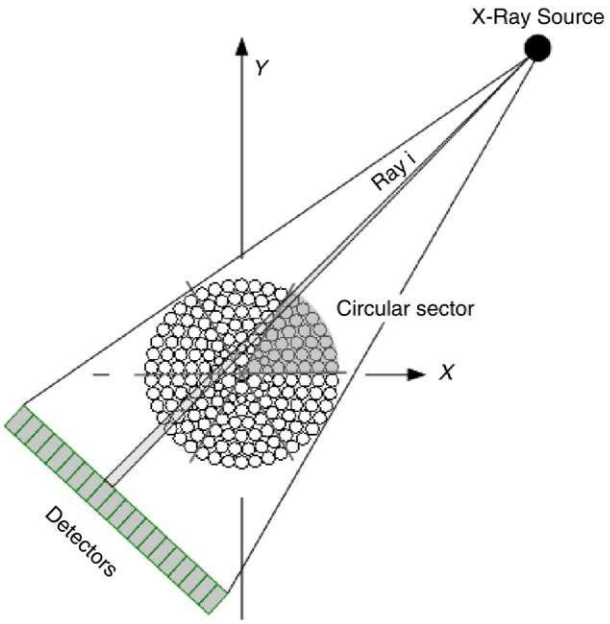

Fig. 4. Polar pixel grid for an example of scanner geometry of six rotated positions.

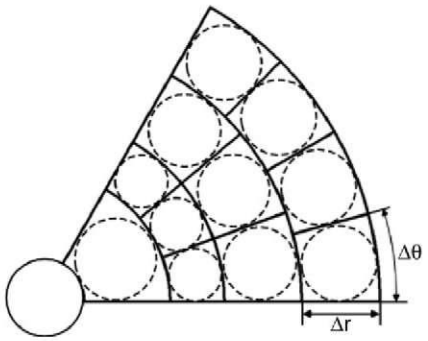

Fig. 5. Example of polar pixel grid in a circular sector. Notice that the circumscribed circles inside the polar pixels, satisfy rules (1) and (2) and are used to set the $\triangle\theta$ polar pixel measure.

scanner focus, in each view, is always the same. In this way, the pixel grid design keeps all the natural symmetries of the system.

The pixel division within the circular sectors has been arranged using the following rules:

(1) A circular pixel, whose diameter is half of the intrinsic spatial resolution of the scanner, is placed on the center of the FOV (isocenter).
(2) From the central circle the rest of the circular sector is divided into polar pixels that are determined by $\triangle r$ and $\triangle\theta$ where:
   (a) All the polar pixels have a circle circumscribed whose diameter is less than or equal to half of the spatial resolution of the system.
   (b) All the circumscribed circles whose centers have the same radial coordinate, have the same diameter.
   (c) $\triangle r$ is the diameter of the circumscribed circles and it is the biggest possible one which accomplishes conditions (a) and (b).

Fig. 5 shows an example of one circular sector. It can be observed a variable size of the polar pixels depending on its distance to the isocenter, as well as an increment of the pixel number on the central area of the FOV due to the design of the pixels within circular sectors. This higher density of pixels implies a higher resolution in the central area where there is located the most quantity of measured target. In this area the scanner sensibility is higher.

4.2. System matrix structure

In ART, the reconstruction problem is defined by a linear equation system

$$WX = P,$$

where W is the SM that models the relation between pixels X and projections P. The vector of projections can be decomposed into a set of N views (P_i), where each P_i acts on all the pixels of the FOV. As we have seen before, since the FOV is splitting into N equal circular sectors, W in the polar grid approach can be decomposed into N submatrices W_i, which affects each P_i component. Therefore, the W_i are obtained by rotating the pixels of each circular sectors and keeping the natural symmetries of the scanner. Consequently, W can be expressed as a block matrix where the first block is the first view W_1 and the rest are rotations of it, that is,

$$W = \begin{bmatrix} W_1 \\ W_2 \\ \vdots \\ W_N \end{bmatrix} = \begin{bmatrix} W_1 \\ RW_1 \\ \vdots \\ R^{N-1}W_1 \end{bmatrix},$$

where R and its powers are the rotations. Furthermore, the rays of each view are symmetric with respect to the line that goes from the focus to the center of the FOV. Therefore, only the first half of beams of the first view needs to be calculated because the second half can be obtained by reflecting the SM data of the first one. Then, if

$$M = \begin{bmatrix} 0 & \cdots & 1 \\ \vdots & \iddots & \vdots \\ 1 & \cdots & 0 \end{bmatrix},$$

we obtain that

$$W_1 = [w, wM],$$

where w is the block matrix corresponding to the first half of beams of the first view. Therefore,

$$W = \begin{bmatrix} w & wM \\ Rw & RwM \\ \vdots & \vdots \\ R^{N-1}w & R^{N-1}wM \end{bmatrix},$$

where w is the only block matrix to be computed.

4.3. Image visualization

The reconstructed images are arranged in a polar configuration and it is necessary to design an additional procedure to display them. We have implemented a viewer that converts a reconstructed image in circular pixels to another in square pixels. The viewer consists of placing each pixel on a cartesian grid thin enough to keep the resolution of the original circular images. The relation between these two grids is calculated as the intersection between them. Moreover, the uncovered areas among circular pixels are filled using nearest neighbor interpolation. The viewer procedure takes only 3 s to convert a polar grid image from a data acquisition of 512 rays to a square pixel image of 2048 × 2048 pixels and does not need any stored data or precalculated information. The converted reconstructed image is reduced in order to compare with the original phantom image. After the conversion from polar pixels to cartesian pixels no post-filter processes are used.

5. Reconstruction algorithm: MLEM

The maximum likelihood expectation maximization (MLEM) algorithm for transmission tomography is one of the most well-known statistical iterative reconstruction methods [6]. Since Poisson noise has been proved to be the

dominating noise contributor [3], this algorithm treats the transmission data as realizations from a Poisson distribution. Therefore, MLEM seeks to maximize the logarithm of the Poisson likelihood objective function,

$$f_j^{k+1} = f_j^k + \frac{\alpha}{m}\left(1 - \frac{\sum_{i=1}^{m} W_{ij}\, p_i}{\sum_{i=1}^{m} W_{ij} b_i \exp(-\sum_{\tilde{j}=1}^{n} W_{i\tilde{j}} f_{\tilde{j}}^k)}\right)$$

where $f = \{f_i | i = 1, \ldots, m\}$ is a vector of the m pixel values of the image, $p = \{p_j | j = 1, \ldots, n\}$ are the n projection values of the data acquisition, b_i is blank scan value at i and $W = \{W_{ij}\}$ is the $m \times n$ SM that gives the percentage of a ray i passing through a pixel j. f^{k+1} is the $k+1$ estimation of the image and the f^0 estimation is usually $f_j^0 = 0, \forall j$.

MLEM was chosen for reconstruction because it can be easily adapted to the peculiarities of both configurations of pixels and it has remarkable properties:

- The iterates f^k converge for $k \to \infty$ to an image that maximizes the loglikelihood.
- The cost of the algorithm increases monotonically with iterations.
- It is easy to incorporate *a priori* information in the algorithm.
- The robustness of the numerical procedure has been established [18].

Two versions of the MLEM were implemented for each grid configuration.

In the square pixel model algorithm, the total matrix has to be computed for all the views of the scanner. For computational reasons we need to calculate the SM in advance and then to store it. Since the complete SM is huge, this process involves a slow access to the data and a slow reconstruction algorithm. The process of generation of the matrix is costly and does not allow us to change the matrix configuration easily.

In the polar pixel MLEM version, as we can see in Section 4.2, the grid has as many identical circular sectors as angular positions of the detector so that, the algorithm uses only the first view and calculates the rest of the views from it by using rotations and reflections.

Moreover, the pixel numeration increases in the same direction as the rotation of the scanner. Since obtaining the corresponding pixels and rays in the rest of views from the first view, is a very easy task, this procedure is carried out by using two permutation matrices whose elements are computed when and only if they are necessary. Therefore, these permutation matrices do not need to be precalculated in advance and the procedure to obtain the matrix elements from the submatrix does not add a high complexity to the algorithm.

The geometry of the pixels and the arrangement on circular sectors allow the entire matrix to be computed from only one position of the scanner. The size of the matrix is decreased as many times as the number of rotations and the time of SM generation is highly reduced too.

6. Experiments for model assessment

6.1. Data source

The simulated projections are a 2D Shepp–Logan head phantom [5] with well-known properties which is widely used in order to validate reconstruction algorithms. The Shepp–Logan phantom contain ellipses with different absorption properties, that resemble the outline of a head. The simulations were built with the Open Source Computer Tomography Simulator package CTSim [17]. An equilinear fan-beam configuration with a fan-beam angle of 20.25° was simulated. Projection data contain 400 views acquired over 360° and each view contains 512 rays. The measures of these models were 35.16 cm × 35.16 cm with a pixel dimension of 6.86 mm. An image of the phantom is shown in Fig. 6. The simulated dimensions of the phantoms and matrix implementations are based on the CT scanner of the *Hospital Clínico Universitario* of Valencia which is a CT-Simulator Metaserto with a Kermath tomography system attached.

6.2. *Figures of Merit*

The assessment of the image quality has been made by comparing the reconstructed images to the simulated phantom using several Figures of Merit. The selected Figures of Merit have measured the main characteristics of the images such as the error of the reconstruction from the original images, the correlation between the phantom and the reconstructed images, the ratio between reconstructed images and the noise, which is approximated as the error between the phantom and the images, and the contrast and homogeneity observed between local areas of the images. The most significative Figures of Merit for studying these aspects have been the following:

- Root Mean Square Error (RMS),

$$\mathrm{RMS} = \frac{1}{N}\sum_{i=1}^{N} \|x_i^r - x_i^o\|$$

  where N is the number of pixels, x^o is the original phantom image and x^r is the reconstructed image.
- Correlation Coefficient (CC),

$$\mathrm{CC} = \frac{1}{N}\frac{\sum_{i=1}^{N}(x_i^r - \bar{x}^r)(x_i^o - \bar{x}^o)}{\sigma_{x^r}\sigma_{x^o}}$$

  where the $\bar{x}^r$ and $\bar{x}^o$ are respectively the mean pixel value of the reconstructed and original images and the σ_{x^r} and σ_{x^o} are their standard deviation values.
- Signal-to-Noise Ratio (SNR),

$$\mathrm{SNR} = \frac{\sum_{i=1}^{N} \|x_i^o\|^2}{\sum_{i=1}^{N} \|x_i^r - x_i^o\|^2}$$

  where the noise component is approximated as the squared difference between the original phantom and the reconstructed image pixels.
- Contrast is defined on specific regions of interest (ROI) by,

$$\mathrm{Contrast} = \frac{|L_B - L_A|}{|L_B + L_A|}$$

  where L_A and L_B represent respectively the average pixel value in ROI A and ROI B.
- CV is defined on each ROI by,

$$\mathrm{CV} = \frac{\sigma_{x^r_{\mathrm{ROI}}}}{\bar{x}^r_{\mathrm{ROI}}}$$

  where the standard deviation and the mean pixel value are calculated from ROI A or ROI B.

RMS, CC and SNR yield a global indicator and Contrast and CV show the behavior in local regions, ROI A and ROI B. The location of the selected ROIs are indicated by dashed ellipses in Fig. 6. Figures of Merit compare the original phantom in Fig. 6 to the reconstructed images without any filtered procedure.

7. Results

The reconstruction provided by the polar pixel model and the square pixel model have been compared in two aspects, matrix efficiency and image quality. Both matrices have been implemented for the geometry of a real CT scanner with a configuration of 512 rays. The most outstanding features of these implementations are summarized in Table 1.

As can be seen in Table 1, polar pixel matrix and square pixel matrix have similar sparsity, but the polar pixel configuration requires a higher number of pixels than its equivalent square pixel one. Despite the increment in the pixel number, the polar grid model makes possible a more compact SM design and allows us to reduce the number

Fig. 6. Shepp–Logan phantom of 512×512 pixels. This model has been generated by means of the Open Source Computed Tomography Simulator package, CTSim [17].

Table 1
The main features of the polar pixel SM and square pixel SM implementation for the specific scanner geometry of the *Hospital Clínico Universitario* of Valencia CT-Simulator (512 rays' configuration)

SM features	Polar pixel	Square pixel
Sparsity (%)	0.2746	0.3627
Pixel number	1 135 201	262 144
Non-zero elements	1 596 106	194 738 088
Size	24.35 Mb	2903.6 Mb
Symmetry reduction factor	800	4
Time of generation	4 s	18 h 45 min 3 s
Time of reconstruction	3 min 3 s	4 min 19 s
Time of visualization	3 s	0 s

The experimental values are given by means of a Pentium 4 CPU 3.2 GHz of 32 bits and 2 GB RAM.

of non-zero elements needed. Therefore, the polar pixel model has a smaller size SM whose generation time is only 4 s. SM usually is computed only once and it is stored and loaded each time that it is needed. However, if the time of generation is highly reduced, SM can be calculated on-the-fly, if and only if the elements are necessary [19]. The effectiveness of this option depends on the elements needed on each measurement, but this is the most efficient alternative without loss of information and allows a flexible model in which the SM adapts to changes easily. The use of symmetries in the reconstruction algorithm for the polar pixel model does not affect the efficiency of the algorithm iterations because it is performed using two simple permutation matrices. In fact, the reconstruction time of the polar pixel case is 1 min 4 s per iteration faster than the square pixel matrix due to the fact of avoiding the computation of much more elements than the square pixel matrix. Table 1 shows that the more complex polar pixel model allows us a more computational efficiency than the square pixel configuration in storage, time of SM generation and time per iteration. A sample of the reconstructed images of the Shepp–Logan phantom are shown in Fig. 7 for the iteration number 50. Fig. 8 shows that both reconstructed images are highly similar and both of them are very close to the original phantom. The reconstructed images have smoother transitions than the original phantom but the transitions of the reconstructed images are getting sharper with iterations. Despite these transitions in the reconstructed images, the quality of the reconstruction has enough quality to discriminate the most important areas of the phantom with a few iterations.

The reconstruction quality provided by both matrices has been measured by means of Figures of Merit from the reconstruction of simulated phantoms. Fig. 9(a) and (b) shows the average RMS and the CC as a function of iteration number. These graphs show that there are negligible differences between the polar pixel model and the square pixel model reconstructions in quality. Nevertheless, from the iteration number 20, the reconstructed images in both cases are highly similar to the original phantom with regard to a small error and a good correlation with the original phantom. On the contrary, Fig. 9(c) shows that results of SNR are better in the square pixel reconstruction than in the polar pixel model, mainly from the iteration number 30. A higher SNR implies that the level of the reconstructed images are

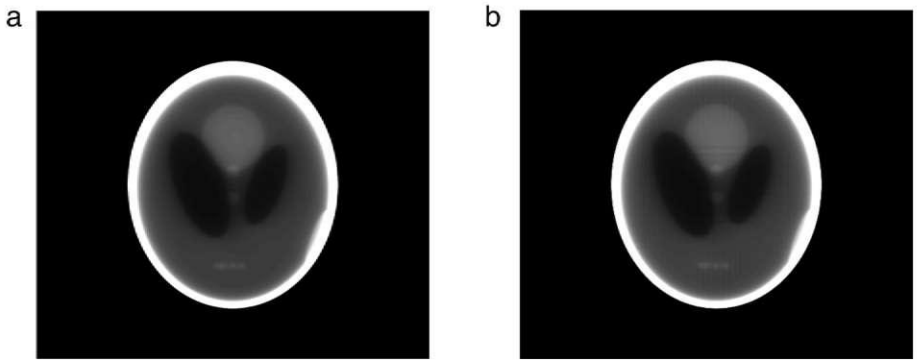

Fig. 7. Iteration number 50 of the Shepp–Logan phantom by means of the polar pixel model (Fig. (a)) and the square pixel model (Fig. (b)).

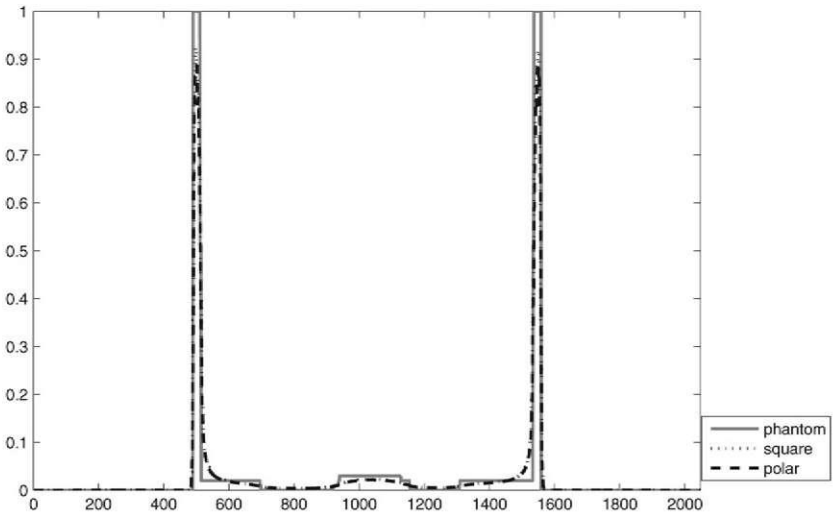

Fig. 8. The figure shows superposed profiles of the two reconstructed images in Fig. 7(a) and (b) and the original Shepp–Logan phantom (Fig. 6).

much more predominant than the noise which can exist in the reconstruction. The polar pixel reconstruction SNR is progressing in a stable SNR until iteration number 65 and then SNR is becoming worse with iterations while the square pixel reconstruction SNR is maintained in a stable ratio. Fig. 9(d) shows the contrast between ROI A and ROI B and it can be seen that the contrast tends to 0.7 and it grows with iterations to the same level in both models. Fig. 9(e) and (f) shows CV for the ROI regions as a function of iteration number. In both ROIs, the variation increases monotonically as a function of iteration number. CV evaluation shows that the homogeneity of the ROI regions is better in the polar pixel model than in the square pixel model, specially for the ROI B case. Finally, we can show in the complete Fig. 9 that the two approaches seem to provide enough quality images and their RMS, CC, SNR, contrast and CV of the polar pixel model reconstructed images are quite similar to the square pixel model ones.

8. Discussion and conclusions

The polar pixel model is more complex than the traditional square pixel one, because it has polar pixel arrangements from circular sectors that require a higher number of pixels than the equivalent square pixel one and needs a visualization procedure. However, the polar pixel model allows us to take advantage of all the natural symmetries of the scanner geometry. Actually, the final number of needed elements is fewer than the square pixel model. Therefore the generation time of the SM is highly reduced to only a few seconds.

The polar pixel model becomes a more compact SM that implies a faster reconstruction algorithm than the square pixel model. Since the procedure to take advantage of the model symmetries is carried out using only two simple

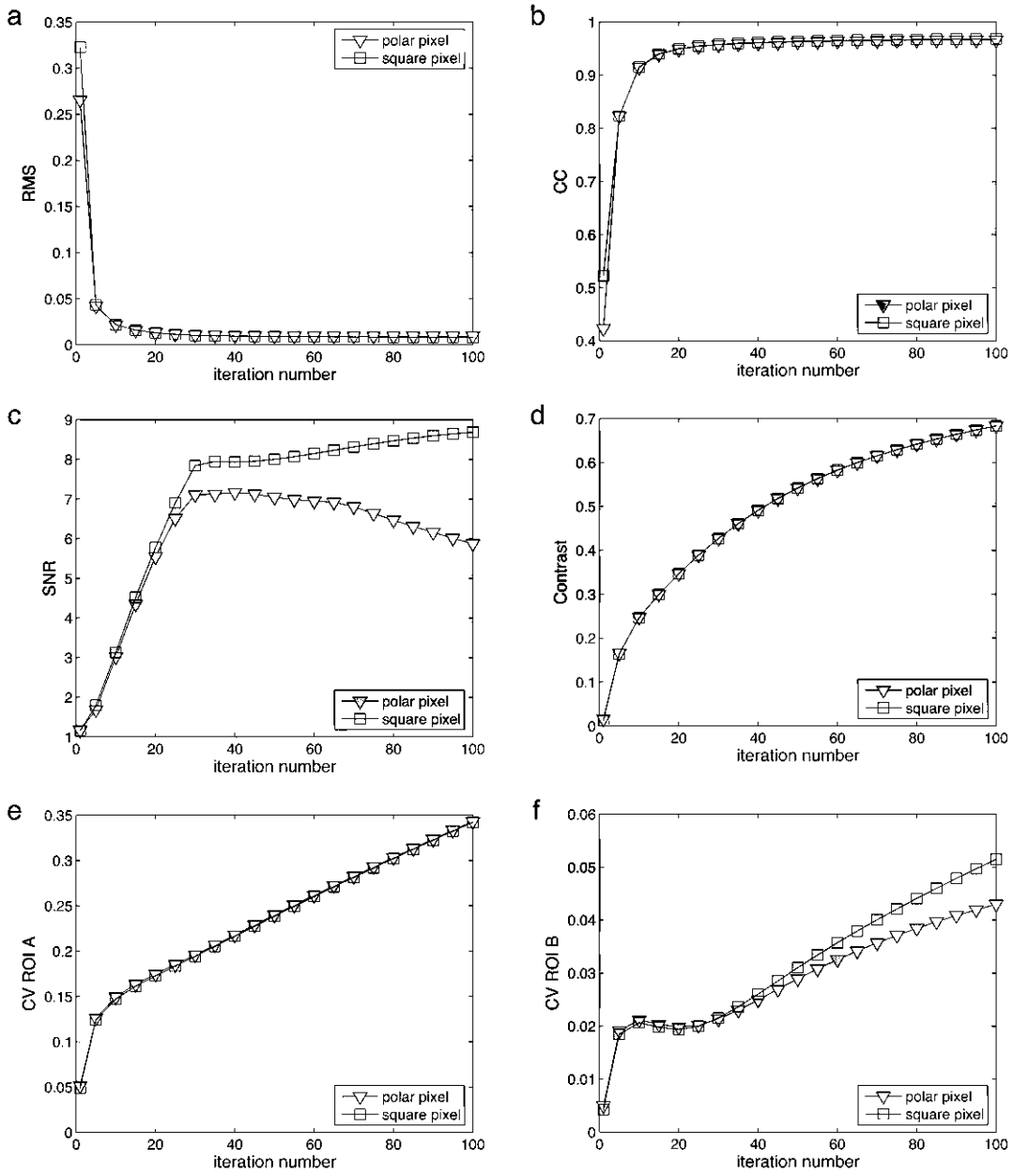

Fig. 9. Figure of Merit of the Shepp–Logan reconstruction from the polar pixel model and the square pixel model implementations on several iterations.

matrices of reflection and rotation, the polar pixel model does not add a high complexity to the reconstruction algorithm.

The visualization procedure developed takes a few seconds to convert the polar pixel images to square pixel and does not need any precalculated information for the conversion. Moreover, this procedure provides quality images avoiding polar artifacts.

The Figures of Merit obtained from the reconstruction of the Shepp–Logan phantom shows that the polar pixel model provides a quality image with similar mean error, correlation, signal–noise ratio, contrast and local variation than the square pixel approach.

Finally, we conclude that the polar pixel model is more efficient than the square pixel model for real scanner geometry implementation conditions and the accuracy of the reconstructed images is equivalent to the square pixel model reconstructed images.

The evaluation of the reconstruction methods using real measurements with noise and a 3D scanner geometry will be part of our study. Moreover, the temporary measures provided by the MLEM algorithm has an important reduction due to the employment of the polar pixel model but, the time per iteration is still too high for practical applications. Therefore, an optimized implementation of the MLEM or alternative reconstruction strategies will be part of our work in the near future.

References

[1] S.C.B. Lo, Strip and line path integrals with a square pixel matrix: A unified theory for computational CT projections, IEEE Trans. Med. Imaging 7 (4) (1998) 355–363.

[2] A.C. Kak, M. Slaney, Principles of Computerized Tomographic Imaging, IEEE Press, 1988.

[3] H. Guan, R. Gordon, Computed tomography using algebraic reconstruction techniques (ARTs) with different projection access schemes: A comparison study under practical situations, Phys. Med. Biol. 41 (1996) 1727–1743.

[4] R.G. Wells, M.A. King, P.H. Simkin, P.F. Judy, A.B. Brill, H.C. Gifford, R. Licho, P.H. Pretorius, P.B. Schneider, D.W. Seldin, Comparing filtered backprojection and ordered-subsets expectation maximization for small-lesion detection and localization in 67ga SPECT, J. Nucl. Med. 41 (2000) 1391–1399.

[5] L.A. Shepp, Y. Vardi, Maximum likelihood reconstruction for emission tomography, IEEE Trans. Med. Imaging 1 (2) (1982) 113–122.

[6] K. Lange, R. Carson, EM reconstruction algorithms for emission and transmission tomography, J. Comput. Assist. Tomogr. 8 (1984) 306–316.

[7] H.M. Hudson, R.S. Larkin, Accelerated image reconstruction using ordered subset of projection data, IEEE Trans. Med. Imaging 13 (4) (1994) 601–609.

[8] T. Hebert, R. Leahy, M. Singh, Fast MLE for SPECT using an intermediate polar representation and a stopping criterion, IEEE Trans. Med. Imaging 22 (5) (1988) 615–619.

[9] C. Mora, M. Rafecas, Polar pixels for high resolution small animal PET, USA, San Diego, Nov. 2006, IEEE NSS-MIC Conf. Rec.

[10] S. Matej, R.M. Lewitt, Efficient 3D grids for image reconstruction using spherically-symmetric volume elements, IEEE Trans. Nucl. Sci. 42 (4) (1995) 1361–1370.

[11] Y.L. Hsieh, G.T. Gullberg, G.L. Zeng, R.H. Huesman, Image reconstruction using a generalized natural pixel basis, IEEE Trans. Nucl. Sci. 43 (4) (1996) 2306–2319.

[12] Y.L. Hsieh, G.T. Gullberg, G.L. Zeng, R.H. Huesman, Projection space image reconstruction using strip functions to calculate pixels more natural for modeling the geometric response of the SPECT collimator, IEEE Trans. Med. Imaging 17 (1) (1998) 24–44.

[13] A.C. Sauve, A.O. Hero, W.L. Rogers, S.J. Wilderman, N.H. Clinthorne, 3D image reconstruction for a compton SPECT camera model, IEEE Trans. Nucl. Sci. 46 (6) (1999) 2075–2084.

[14] V. Israel-Jost, P. Choquet, S. Salmon, C. Blondet, E. Sonnendrücker, A. Constantinesco, Pinhole SPECT imaging: Compact projection/backprojection operator for efficient algebraic reconstruction, IEEE Trans. Med. Imaging 25 (2) (2006) 158–167.

[15] R. Bevilacqua, E. Bozzo, O. Menchi, Comparison of four natural pixel bases for SPECT imaging, J. Comput. Appl. Math. 198 (2) (2007) 361–377.

[16] L. Jian, L. Litaoa, C. Penga, S. Gia, W. Zhifang, Rotating polar-coordinate ART applied in industrial CT image reconstruction, NDT E Int. 40 (4) (2007) 333–336.

[17] The open source computed tomography simulator: http://ctsim.org/, Last Access Feb. 2006.

[18] J. Nuyts, B. De Man, P. Dupont, M. Defrise, P. Suetens, L. Mortelmans, Iterative reconstruction for helical CT: A simulation study, Phys. Med. Biol. 43 (1998) 729–737.

[19] H. Kudrolli, W. Worstell, V. Zavarzin, SS3D Fast 3D PET iterative reconstruction using stochastic sampling, IEEE Trans. Nucl. Sci. 49 (1) (2002) 124–130.